Can Weak Gravitational Lensing Determine Matter Halo Fall-Off For Clusters Of Galaxies?

Abstract:

The ability for weak lensing observations to constrain the commonly used Navarro, Frenk and White (NFW) density profile for galaxy clusters was examined by creating "mock" data similar to current or near future telescope capabilities and attempting to reconstruct the NFW density parameters as one would in practice. The shearing and magnification of images distorted by weak gravitational lensing was derived by integrating the geodesic deviation and optical scalar equations along the null geodesics connecting the observer to a distant source. We determined the level of expected accuracy of lensing to recover lens profile parameters in current measurements by performing a Monte Carlo simulation of the data. We find a large spread in parameters values, all clustered around the corrected total mass. Also, we find that current and near future telescope capabilities cannot constrain the lens profile truncation mechanism. The lens profile truncation mechanism will be well constrained by future telescope with approximately less than 10% of the current error levels in the averaged observed ellipticity. This implies a significant advance in telescope technology will be required in reducing the atmospheric effects and telescope mirror and CCD errors that cause the observed images to be smeared relative to the "true sky" before weak lensing observations can tell us how galaxy cluster mass density is truncated.

I. Introduction

Galaxies are usually not found randomly dispersed in the universe. Most of them are part of groups of 10-50 clusters or more (sometimes much more). This has to do with how galaxies form to begin with. Our best understanding is that very early in the universe's history, the universe was filled with billions of photons, hydrogen atoms, helium and very little other normal matter. Also, there was a lot of dark matter, which we do not know much about other than that it is gravitating matter that is hard to detect. Most of these elements were smoothly spread out, almost perfectly evenly across the entire universe. But there were very, very small perturbations in the density. Those perturbations collapsed due to gravitational attraction. The process that led to small perturbations to become bigger and bigger clumps led to forming stars, then galaxies, and then clumps of galaxies. Most of the matter ended up in groups, clusters of galaxies, just by naturally following the gravitational attraction of matter on itself.

We can do numerical simulations of this process. On average, what happens is that we get a spherical matter distribution with a density ρ_{nfw} which is the density found by Navarro, Frenk, and White (NFW density profile). When we look at actual galaxies and clusters of galaxies, they do indeed appear to follow the NFW profile on average.

However, there is a problem. If we try to integrate the total mass of the NFW profile

$$M = 4\pi \int_0^\infty r^2 \rho_{NFW} dr \qquad (1)$$

We find that the total mass of an NFW profile is infinite. It needs to be finite, however, because one clump of matter cannot have infinite mass.

So somehow the numerical simulations that track these particles in the work of NFW go astray at large radii. What we have to do is "truncate" the NFW profile, by multiplying it by a factor that is close to 1 at "small" radii but it is $1/r^2$ or more at large radii.

Figure1: Yellow blobs are the clusters and blue ellipses are same galaxy multiply imaged. See how shape differs but it is always elliptical and oriented tangent to a circle.

Gravitational lensing is a phenomenon that occurs when an object, like a cluster of galaxies, acts as a lens between the light source and the observer. For instance, when light comes from a source and travels past galaxies or clusters of galaxies between the light source and the observer, it bends to follow the path of the curvature of space caused by the warping of space-time. Hence, gravitational lensing probes the distribution of matter in a galaxy or cluster. In particular, the appearance of background galaxies is distorted by the gravity of the cluster. How much bending or distortion we see tells us

about the mass and mass distribution of the lens. The same thing is true for an object you look at behind a piece of glass. If the object has a shape you know, when you look at it through the glass, you can tell how the glass is shaped.

General relativity, which states that the presence of any mass bends the path of light passing near it, consequently leads to the production of the giant arcs and multiple images associated with strong gravitational lensing. But most lines of sight in the universe are in the weak lensing regime where the effects of general relativity are very small. In the weak lensing regime, the distribution is impossible to detect in a single background source. However, if we average over many background sources, we can still detect the presence of lensing as a systematically alignment of the background source shapes around the lensing mass. Thus, weak gravitational lensing is a statistical measurement.

Observational weak lensing is a major area of research where the mass properties, including the total mass and mass density profile, are measured from the distortion of shapes of distant galaxies behind the lens. In the present work, I investigate if weak gravitational lensing observations can tell how the matter distribution of a cluster of galaxies is truncated. I do this be creating "mock" data with noise that simulates current or future weak gravitational lensing observations and reconstructing the parameters that model the lens's matter distribution.

II. Methods

A particular lensing situation involves setting a hypothetical lens at a certain redshift and fixing parameters of model -- including how the lens is truncated. This will

enable us to compute the "true" distortion due to this lens. We can then add noise to our true shape that simulates the typical error in real observations. The amount of noise we add will depend on assumptions we will make about the seeing of future telescopes and the number of background galaxies that future telescopes will detect.

After adding noise, we will attempt to fit "signal plus noise" to a truncated NFW model's prediction (try to find parameters that we set initially). In the absence of adding noise, we can recover the initial parameters exactly. But with the noise that we added to model observational error, there will be a range of parameters that provide "good" fits to the data.

After fitting signal plus noise, we are ready to examine how well constrained these models are. An important question for us is whether the fits to the simulated weak lensing observations are very good -- tightly constrain the possible model parameters -- or not.

III. Weak Lensing Equations

Numerical modeling of dark matter haloes, as found in Navarro et al. 1997, predicts a density of the form

$$\frac{\rho(r)}{\rho_{crit}} = \frac{\delta_c}{\left(\frac{r}{rs}\right)\left(1+\frac{r}{rs}\right)^2}\ , \tag{2}$$

which is also known as the NFW model. Here, ρ_{crit} is the critical density given by

$$\rho_{crit} = \frac{3H(z)^2}{8\pi G}, \tag{3}$$

in terms of the gravitational constant and Hubble's constant at the lens redshift, r_s, is a scale radius defined as the peak of $r^2\rho(r)$ and is a characteristic radius of the cluster. We take the Hubble constant $H_0 = 70$ km/s/Mpc, the matter density $\Omega_\wedge = 0.7 = 1 - \Omega_m$. Here, δ_c is a characteristic over density for the halo, and ρ_{crit} is the critical density for closure of the universe at the redshift, z, of the halo, $H(z)$ is at the same redshift, and G is Newton's constant [6]. A "virial" radius is defined as the radius r_{200} of the sphere with mean density equal to $200\rho_{crit}$.

In our numerical simulations, we use c as the halo's concentration and it's defined as $r_{200}/r_s \equiv c$. This concentration parameter is related to the characteristic density contrast by

$$\delta_c = \frac{200}{3}\frac{c^3}{\log(1+c) - c/(1+c)}. \tag{4}$$

For our modeling we take $r_s = 0.25$ Mpc, $c = 7.31505$ and set $\tau = 3c$ which ensures good agreement between the NFW model and the truncated NFW model within the virial radius [6]. We place the lens at $z_s = 0.25796$, and the total mass for this parameter choice is 2.0×10^{15} solar masses. We find an average background redshift of all the sources to compute the projected matter density by specifying an average D_s, D_l, and D_{ls} in $\sum_{crit}$. This is because the measured gravitational shear is directly related to the dimensionless projected matter density $k(\theta)$, given by

$$\sum_{crit} = \frac{c^2 D_s}{4\pi G D_l D_{ls}}. \tag{5}$$

In this case, it applies for angular diameter distances to the lens, source, and between the lens and source [6]. Consequently, the lens mapping depends on the bending angle, which is the gradient of the projected gravitational potential. Thus, the Jacobian of the lens mapping

$$\mathrm{A} = \begin{pmatrix} 1-\kappa-\gamma_1 & -\gamma_2 \\ -\gamma_2 & 1-\kappa+\gamma_1 \end{pmatrix}, \tag{6}$$

controls weak lensing image distortion. The strategy then is to use the inverse Jacobian matrix, A^{-1}, to map small vectors from the source plane to the lens plane or image plane. The fact that the two eigenvalues of A will be different in general implies that a circular source will be imaged, to first approximation, into an ellipse.

The eigenvalues of A are $1-k\pm|\gamma|$. The axis ratio of the elliptical image of a circular source is given by the ratio of these two eigenvalues. Acting on a circular background source with certain radius, lensing generates an ellipse with major and minor axes as long as the shear and convergence do not change over the size of the source. The eigenvectors of the matrix indicate the directions of stretching and contraction due to lensing, and the eigenvalues give the magnitudes of the lengths of the semi-axes [6]. The formation of a circular source with unit area is mapped into an ellipse when setting $\gamma = \sqrt{\gamma_1^2 + \gamma_2^{\,2}}$. The ellipse then has a unit area of

$$A_{tl} = \left| \frac{1}{(1-\kappa)^2 - \gamma^2} \right|, \tag{7}$$

and the ratio of the semi-axes is

$$R_{tl} = \left| \frac{1 - \kappa + \gamma}{1 - \kappa - \gamma} \right|. \tag{8}$$

If the matter distribution is axially symmetric, then

$$\gamma(x) = \frac{\overline{\Sigma}(x) - \Sigma(x)}{\Sigma_{crit}} \tag{9}$$

where $\overline{\Sigma}(x)$ is the average projected mass density inside a circle of radius x. For this particular lensing simulation, we use the expression for the projected mass densities and γ as prescribed by Baltz et al [6].

VI. Noise

In the presence of convergence and shear, a circular source becomes elliptical in shape. The convergence term magnifies the background objects by increasing their size, and the shear term stretches them. The ellipticity, ε, is defined in terms of the ratio of the semi-minor to semi-major axes, and it is given by

$$\varepsilon = \frac{1 - 1/ratio}{1 + 1/ratio} \,. \tag{10}$$

To measure the tangential alignment around the foreground mass caused by the convergence and shear, it is necessary to measure the ellipticity of individual images and construct a statistical estimate of their systematic alignment. That is, if we average over the ellipticity of images predicted by the thin lens approximation we can detect the presence of lensing as a systematically alignment of the background source shapes around the lensng mass.

To average ellipticity measurements, we set up annular bins with equal width that in some way cover the shape of the cluster. The error that we observe in the averaged observed ellipticity is estimated by the number of objects averaged over and the intrinsic ellipticity dispersion, σ_ε, as $\sigma = \sigma_\varepsilon / \sqrt{N}$. Typical values of σ_ε are about 0.3 [4], which accounts for the instrumental and atmospheric effects that cause the observed images to be smeared relative to the "true sky". Thus, we set up fifteen annular bins of equal width with the center of the first bin at 100-arc sec and the center of the last bin at 600-arc sec, which corresponds to typical dithering of ground-based, wide field telescopes today. We also consider 25 annular bins between 100 and 900 arc sec, which could be done today with different telescope pointing.

In the Navarro, Frenk and White (NFW) profile, it is convenient to define $x = r / r_s$, in order to get the NFW profile in a simpler form. The truncated version of the NFW model proposed by Baltz is

$$\rho(x) = \frac{M_0}{4\pi r_s^3} \frac{1}{x(1+x)^2} \frac{\tau^2}{\tau^2 + x^2}. \tag{11}$$

Here, we define the truncation radius to be a factor of τ larger than the scale radius.

For the purposes of our weak lensing simulations, we are interested in the projected mass density. We first define the function

$$F(x) = \begin{cases} \dfrac{\cos^{-1}(1/x)}{\sqrt{x^2 - 1}} & x > 1 \\ \dfrac{Log\left[(1/x) + \sqrt{(1/x)^2 - 1}\right]}{\sqrt{1 - x^2}} & x < 1 \end{cases}. \tag{12}$$

We also define the following logarithm,

$$L(x) = Log\left[\frac{\sqrt{\tau^2 + x^2} - 1}{x}\right]. \tag{13}$$

With these definitions, the projected surface mass density is given by [6]

$$\sum(x) = \frac{M_0}{r_s^2}\frac{\tau^2}{2\pi(\tau^2+1)^2}\left\{\frac{\tau^2+1}{x^2-1}[1-F(x)] + 2F(x) - \frac{\pi}{\sqrt{\tau^2+x^2}} + \frac{\tau^2-1}{\tau\sqrt{\tau^2+x^2}}L(x)\right\}. \tag{14}$$

The strategy then is to derive the convergence, κ, the shear, γ, and get the projected mass. We can derive κ by taking $\kappa = \sum/\sum_{crit}$. The projected mass inside radius x, is

$$M_{proj}(x) = M_0\frac{\tau^2}{(\tau^2+1)^2}\left\{[\tau^2+1+2(x^2-1)]F(x) + \tau\pi + (\tau^2-1)\ln\tau + \sqrt{\tau^2+x^2}\left[-\pi + \frac{\tau^2-1}{\tau}L(x)\right]\right\}$$

To derive the shear, we use the mean projected surface density inside radius x, which is $\overline{\sum} = M_{proj}/\pi r^2$. If we define $\Gamma = \overline{\sum} - \sum$, the shear then is $\gamma = \Gamma/\sum_{crit}$.

VII. Fitting Noise

Hence, by picking up lens parameters we can model the ellipticity profile using the thin lens approach of image distortion using χ^2 minimization [9]. To this end, we use a Levenberg Marquardt fit based on the implementation in [4]. Thus, let ε_i be the averaged ellipticity measurements (as given by Eq.10) and a_i be the lens parameters which in this case can be (c, r_s) or (c, r_s, τ) if we are fitting for three parameters. The χ^2 function then is

$$\chi^2 = \sum_{i=1}^{N} \left[\frac{\varepsilon_i - \varepsilon(x;a_i)}{\sigma_i} \right]^2, \tag{16}$$

where a_i is the correspondent parameters. Taking its first derivative with respect to the parameter a, we can notice that the first derivative will be zero at the χ^2 minimum and has components

$$\frac{\partial \chi^2}{\partial a_k} = -2 \sum_{i=1}^{N} \frac{[\varepsilon_i - \varepsilon(x_i;a)]}{\sigma_i^{\,2}} \frac{\partial \varepsilon(x_i;a)}{\partial a_k}, \tag{17}$$

For our particular weak lensing simulations, it depends on the set of three unknown parameters, k, where $a_k = 1,2,3.$

VIII. Results

The matter density, with the parameters (c, r_s, τ), is projected into the lens plane and the thin-lens κ and γ is computed. We found that in the absence of adding noise, we recover the initial parameters exactly. Figure 3 shows how much (c, r_s) can vary because of noisy data. Thus, we examined how well constrained NFW profile density model fits are given current telescope capabilities – with the concentration parameter on the vertical axis and the scale radius on the horizontal axis. The shape of this spread is dictated by holding the total mass of the profile roughly constant – highly concentrated but smaller clusters or lower concentration spread out over a larger area.

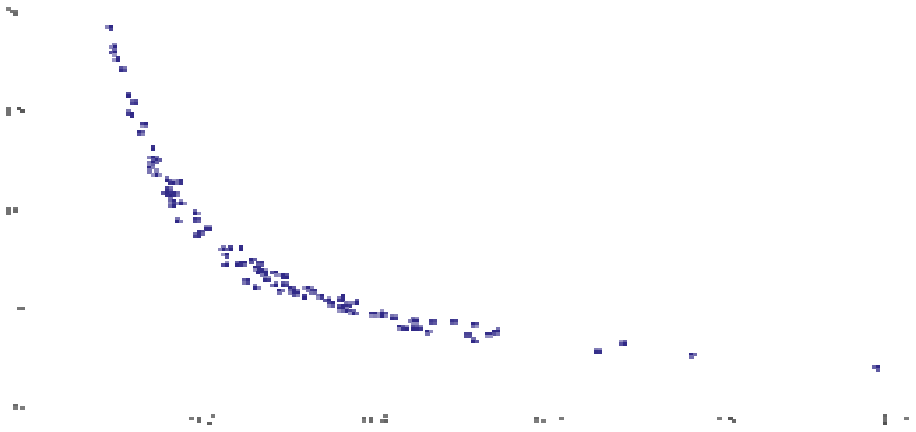

Figure 3: One realization of lensing with 100 different noises. This is 100 examples of noise data where we solve for c and r_s values.

The thin-lens is modeled as a truncated NFW profile with $\tau = 3c$, $r_s = 0.25$ Mpc, $z_s = 0.258$, which ensures good agreement between the NFW model and the truncated NFW model within the virial radius [6]. We place the lens at $z_l = 0.45$, and the total mass inside the virial radius of $2.0 \times 10^{15} M_{\otimes}$ solar mass. The ellipticity and expected uncertainty for fifteen equally spaced annular bins ranging from 100 arc sec to 900 arc sec for 25 simulations is obtained while holding $\tau = 3c$ for the current values. We find that in the absence of any noise (which accounts for the instrumental and atmospheric effects that cause the observed images to be smeared relative to the "true sky"), the lens profile truncation mechanism can be well constrained as shown in figure 4.

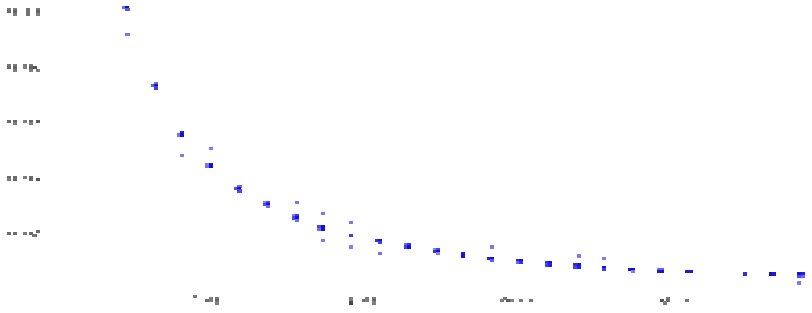

Figure 4: Plot of the thin-lens approximation best fit γ and θ values for $\tau = 3c$ for twenty-five simulations, in the absence of noise. The horizontal axis represents the θ values and the vertical axis represents the γ values.

Using a Levenberg-Marquardt fit based on the implementation in [4], we find the fitting parameters for modeling thin-lens approximation of image distortion. Thus, we picked up lens parameters modeled the ellipticity profile using the thin lens approach of image distortion using χ^2 minimization. The graph of χ^2 versus m in tau = mc is shown in figure 5.

Figure 5: Graph of χ^2 minimization based on the implementation in [4]. No noise in data, and fitting (c, r_s, τ) for $\tau = mc$.

We varied (but hold fixed) $\tau = mc$ to get values of c and r_s on τ plane in an attempt to understand the parameters (c, r_s) on τ. Signal plus noise fit to our NFW model's prediction and truncated NFW model's prediction was investigated, and a range of (τ, r_s, c) parameters that provide "good" fits to the original data is obtained. Figure 5 shows the resulting graph of the attempt of fitting these three parameters to the data. As shown in the graph, while we vary m and fit (c, r_s) there is a minimum in χ^2. Thus, we can fit for (c, r_s, τ) if no noise. We found that we are unable to fit for (τ, r_s, c) at current telescope resolutions. The experiment was repeated over at different noise properties, and

different model parameters in an attempt to understand why we are unable to fit for (τ, r_s, c) at current resolution.

We find that in the presence of current noise, current and near future telescope capabilities cannot constrain the lens profile truncation mechanism. Figure 7 shows the resulting graph of attempting to recover the χ^2 in the presence of current noise. We can notice that with current noise we are not able to obtain a minimum. Nevertheless, we can recover a range of equally good fits to the observational data, as shown in Figure 6.

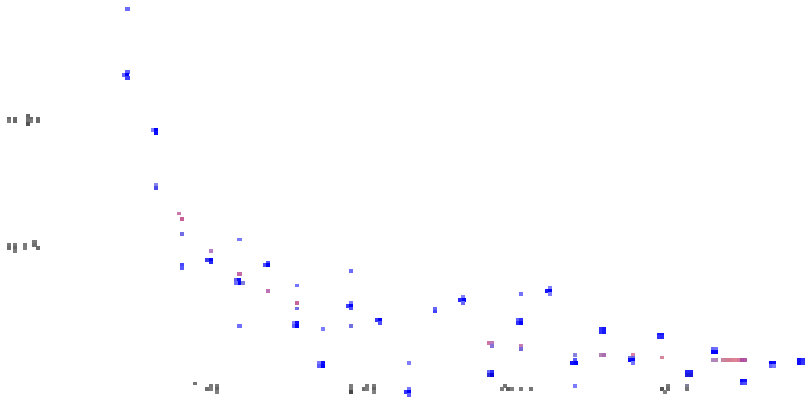

Figure 6: Resulting graph of attempting to fit for parameters (r_s, c, τ). The blue line represents the true data, the red line represents resulting attempt to fit for the three parameters, and the dots and error bars represent the instrumental and atmospheric effects that cause the observed images to be smeared relative to the "true sky". The horizontal axis represents the θ values and the vertical axis represents the γ values.

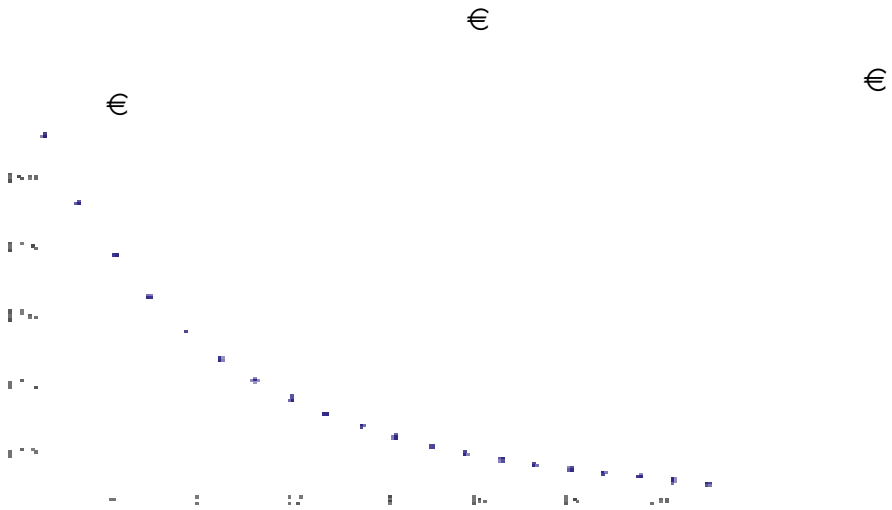

Figure 7: Resulting graph of the attempt to recover the same χ^2 graph as Figure 5, in the presence of current telescope resolution (noise). The horizontal axis represents the values of χ^2, and the vertical axis represents the m values. There was no minimum found.

While we find that we cannot constrain lens truncation with the current telescope resolution, future telescopes with approximate less than 10% ($\sigma_\varepsilon = 0.03$) of the current error that we observe in the averaged observed ellipticity (typically about $\sigma_\varepsilon = 0.3$) may be able to. The number of objects per square arc minute was doubled, and the atmospheric noise was reduced. Figure 8 shows the resulting graph of fitting for parameters when telescope resolution is increased.

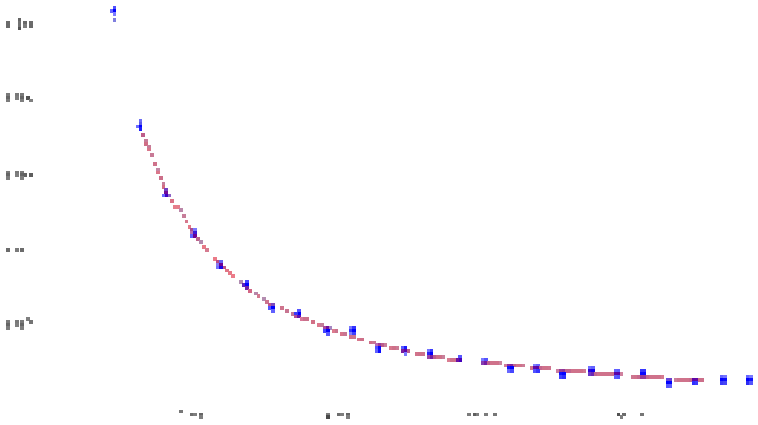

Figure 8: Resulting graph of fitting for parameters when telescope resolution is increased to $\sigma_\varepsilon = 0.03$. The blue line represents the true data, the red line represents resulting attempt to fit for the three parameters, and the dots and error bars represent the instrumental and atmospheric effects that cause the observed images to be smeared relative to the "true sky". The horizontal axis represents the θ values and the vertical axis represents the γ values.

VII. Conclusion

In this paper, we examined the ability for weak lensing observations to constrain lens profile parameters, (c, r_s, τ), in current measurements. We determined the level of expected accuracy of lensing to recover these lens profile parameters by performing a Monte Carlo simulation data and finding a range of parameters that provide "good" fits to the data.

We repeated experiment over at different noise parameters, and different model parameters. We understood that the amount inherited error leads to wide range in (c, r_s) best-fit values. This wide range found in (c, r_s) best fit values imply that it will be hard to fit for (c, r_s, τ). This result leads us to conclude that current and near future telescope capabilities cannot constrain the lens profile truncation mechanism.

Using the thin-lens approximation and a truncated NFW profile that has been projected into the lens plane, and a Levenber-Marquardt fit based on the implementation in [4], we find the best-fit parameters (c, r_s) while varying τ. As showing in these figures, we find very little dependency of parameters (c, r_s) that explains why current and near future telescope capabilities cannot constrain the lens profile truncation mechanism.

Giving these findings, we increased telescope resolution to $\sigma = 0.03$ in an attempt to examine future telescope capabilities to constrain (c, r_s, τ) parameters. We find that the lens profile truncation mechanism will be well constrained by these future telescopes.

References:

[1] Navarro, J. F., Frenk, C. S. & White, S. D.M., "A Universal Density Profile from Hierarchical Clustering." AJP, 490, 493 (1997).

[2] Baltz, E. et al., "Analytic models of plausible gravitational lens potentials." JCAP 0901:015 (2009).

[3] Schneider Peter, "Cosmological Applications of Gravitational Lensing" Max-Planck-Institut Fur Astrophysik, Postfach 153, D-85740 Garching, Germany.

[4] Press et.al. Numerical Recipes The Art of Scientific Computing, 3rd Edition, Cambrigde University Press, Cambridge, 2007.

[5] Kling, T. & Bianchini, L. "Continuous image distortion by astrophysical thick lenses", submitted to General Relativity and Gravitation.

[6] Frittelli, S., Kling T. P., & Newman, E. T., 2001, Phys. Rev. D, 61, 064021.

[7] Schneider, P. et al, Gravitational Lensing: Strong, Weak, and Micro (Springer-Verlay, New York, 2006).

[8] Baltz, E. et al., 2007, cited on May 13, 2011.

[9] Newman, E. T. & Penrose, R., 1962, J. Math Phys. 3, 566-78.